Deciphering the Role of Oxygen in Materials for Heterogeneous Catalysis and Energy Storage: A Dive into the Oxygen K-Edge

Soumya Kumar Das[1,2], Stavros Theofanidis[3], Francesco Giannici[4], Christoph Sahle[1], Mauro Rovezzi[5], Hilde Poelman[2], Vladimir Galvita[2], Dirk Poelman[6], Lorenzo Stievano[7,8], Yves Joly[9], Alessandro Longo*[1,10]

[1] ESRF, The European Synchrotron, 71 Avenue des Martyrs, CS40220, 38043 Grenoble Cedex 9, France

[2] Laboratory for Chemical Technology, Ghent University, Technologiepark 125, 9052 Zwijnaarde, Belgium

[3] AristEng S.à r.l., 77, Rue de Merl, L-2146, Luxembourg City, Luxembourg

[4] Dipartimento di Fisica e Chimica "Emilio Segrè", Università di Palermo, Viale delle Scienze, I-90128 Palermo, Italy

[5]Univ. Grenoble Alpes, CNRS, IRD, Irstea, Météo France, OSUG, FAME, 38000 Grenoble, France

[6] LumiLab, Department of Solid State Sciences, Ghent University, 9000 Ghent, Belgium

[7] Institut Charles Gerhardt Montpellier (ICGM), Univ. Montpellier, CNRS, ENSCM, Montpellier, France

[8] Réseau sur le Stockage Electrochimique de l'Energie (RS2E), CNRS, Amiens, France

[9] Université Grenoble Alpes, CNRS, Institut Néel, F38042 Grenoble, France

[10] Istituto Studio dei Materiali Nanostrutturati-CNR, Consiglio Nazionale delle Ricerche, via Ugo La Malfa 90146 Palermo, Italy

*corresponding author e-mail: alessandro.longo@esrf.fr

Abstract:

Understanding the structural and electronic properties of oxygen in materials is critical for advancing various technological applications, particularly in catalysis and energy storage. Oxygen species play a pivotal role in mediating reactions within metal-oxide systems, significantly influencing the reactivity and stability of catalysts. Insight into the electronic structure of oxygen, comprising hybridization and bonding with transition metals, provides a deeper understanding of catalytic processes and the efficiency of electrocatalysts. Additionally, oxygen's involvement in electrochemical processes within batteries, particularly through anionic redox reactions, underscores its importance in developing efficient energy storage solutions.

This review focuses on the use of two empirical parameters in O K-edge simulations, offering a guide on simulating observed O spectra for oxide solids. By bridging experimental fingerprints with theoretical approaches, an in-depth understanding of the spectra is provided. First, the theory defining the empirical parameters of the FDMNES code, "*dilatorb*" and "*screening*" is presented. Then, the importance of studying the O K-edge is highlighted through discussion of selected case studies. The latter illustrate how oxygen K-edge experiments and simulations are indispensable tools for advancing the understanding of catalytic and energy storage processes and improving materials design by offering detailed information on the electronic structure, bonding, and real-time changes in (electro)catalysts.

I. Introduction

Oxygen plays a pivotal role in many different research areas, such as electrocatalysis, heterogeneous catalysis, and energy storage. The role of oxygen in heterogeneous catalysis is crucial and multifaceted. Various oxygen species, including atomic oxygen (O), di-oxygen (O_2), reactive di-oxygen intermediates (such as superoxide - O_2^- - and peroxide -O_2^{2-}), as well as oxygen incorporated in oxide lattices, participate actively in catalytic processes. These species facilitate the activation and transformation of reactants. Gas-phase oxygen itself can participate in a reaction as oxidant, removing electrons from neighboring atoms, or as reactant, forming new bonds with other elements. This however requires activation of the O_2 molecule, *i.e.* breaking the strong O-O bonds (498 kJ/mol),[1] as an essential step in, for instance, oxidation reactions, where catalysts assist in the O_2 dissociation.[2–4]

In solid oxide lattices, used as heterogeneous catalysts, oxygen serves as a link between the different cationic species, playing a crucial role in mediating the electronic modifications occurring upon chemical treatment. Indeed, the oxygen atoms in the lattice can participate in reaction pathways by facilitating the transfer of oxygen species between the catalyst surface or bulk and adsorbed reactants. In particular, the arrangement of oxygen atoms in the lattice can influence the accessibility and stability of active sites.[5,6] Moreover, oxygen vacancies and other defects significantly impact the catalytic activity. In fact, these material defects provide sites where oxygen adsorption and activation are modified, leading to improved reactivity.

The intricate interaction between oxygen species and catalytic surfaces, including those where oxygen is part of the lattice, enhances the efficiency and selectivity of numerous industrial and environmental processes, contributing to the development of more sustainable

and effective catalytic solutions. For instance, oxygen vacancies in perovskite oxides can enhance catalytic properties by providing sites for oxygen activation and facilitating redox reactions. Similarly, oxygen vacancies in metal oxides like ceria (CeO_2) can enhance their catalytic efficiency by improving oxygen mobility and reactivity.[7] Hence, understanding and controlling the different functions of O is crucial for tailoring catalysts to specific reactions and optimizing their performance.[5–11]

Similarly, oxygen is extremely important in electrochemical or electrocatalytic processes and the performance of batteries, fuel cells, and energy storage materials. The most common positive electrode materials for Li-ion batteries are solid oxides. Oxygen is the major redox-active species in metal-air systems,[12–14] and it participates in the electrochemical processes of Li- and Na-rich layered oxide cathodes through the anionic redox mechanism.[15–18] Oxygen-containing species are also extremely important for the ionic transport properties and stability of solid electrolyte interphases (SEIs),[19–21] as well as in solid electrolytes, where they participate in the ionic conduction through coordination to the moving Li^+ ions.[22,23]

To monitor and unravel the intricate details of the interactions between oxygen and neighboring elements in both catalytic and energy storage systems, adequate O-probing experiments are needed. Given the light character of oxygen, the study of the O X-ray absorption K-edge (~530 eV) has long remained a challenging frontier, often eluding comprehensive investigation due to its complexity, especially in the context of intricate and multifaceted materials. Recently however, different features of the O K-edge as exhibited in several simple and complex oxides have been reported.[24] Oxygen K-edge spectra can reveal changes in metal-oxygen hybridization and bonding, which are essential for understanding the reactivity and efficiency of (electro)catalysts.

To detail oxygen in both catalytic and energy storage systems, researchers apply advanced characterization techniques such as soft X-ray Absorption Spectroscopy (XAS),[25–27] Electron Energy Loss Spectroscopy (EELS),[28,29] Hard X-ray Photoelectron Spectroscopy (HAXPES)[16,30,31] and X-ray Raman Scattering (XRS) spectroscopy.[32–34] Each of these spectroscopic techniques provides complementary information about the structural and electronic properties of oxygen in a material. By employing a combination of these highly sensitive techniques,[35–38] a comprehensive picture of the material's behavior at the O K-edge can be obtained.

The O K-edge XAS corresponds to excitations of the oxygen 1s orbital to empty *p*-type states, offering a window onto the electronic structure and chemical environment of oxygen-containing species within a material. The spectral region above the edge provides unique

information about the unoccupied states - and offers insight into the electronic transitions involving oxygen orbitals. The latter permits understanding the bonding nature and coordination environment of oxygen in a material. The O K-edge XAS is an element- and orbital-specific analytical tool that enables researchers to investigate the role of oxygen in various chemical environments, including (electro)catalytic processes. This specificity is essential because oxygen significantly influences the reactivity and stability of (electro)catalysts. By probing the O K-edge, the atomic and electronic structure of the materials can be determined, elucidating how oxygen atoms and ions interact with surfaces and other elements in the material. These insights are critical for understanding the electronic structure and chemical bonds that underpin (electro)catalytic activity.

Compared to other techniques, XRS offers the significant advantage of measuring the O K-edge using hard X-rays, therefore offering true bulk information. In XRS, the incident X-ray beam interacts with the sample and is scattered inelastically. Accordingly, a momentum of magnitude q and energy (E) are transferred to the sample. For disoriented samples - *e.g.* powders, q is defined as $q=(4\pi/\lambda)\sin\theta$, where 2θ is the total scattering angle and λ the incident X-ray wavelength. The scattered X-ray beam is then analyzed with respect to energy and momentum. Since the choice of the incident energy is not critical, XRS allows the use of high energy (e.g. 10 keV), thereby circumventing the low penetration depth of soft X-rays to study the modifications of the lattice oxygen in the bulk and under in situ conditions. XRS measurement usually takes a long time due to low cross-section and hence requires very high X-ray flux along with a large number of analyzers. However, at low q (i.e. at low scattering angle) XRS becomes equivalent to XAS providing similar information about the electronic structure of the probing element.[39] This information is crucial for developing materials that are applied in catalysis, electrochemical energy storage, and other processes where lattice oxygen plays a prominent role.

Quantitative analysis of the O K-edge data, required to extract structural and electronic information, typically involves theoretical calculations, aiming to reproduce all features of the experimental spectra. Indeed, the O K-edge measured by XAS or XRS can be simulated using the projected Density of State (pDOS) of oxygen and corresponding transition matrix elements can be calculated within Density Functional Theory (DFT). Accordingly, the X-ray spectrum allows for a qualitative analysis without explicit calculations.[24,40,41] The same approach applies to the q-resolved XRS data in different scattering ranges (e.g. low q).[42]

While DFT is the preferred method for understanding and optimizing the electronic and atomic structures of pristine materials, accurately matching calculated and experimental

spectra for materials altered by physicochemical treatments is challenging and time-consuming. Indeed, it requires exploring a wide range of possible atomic arrangements within the studied system.[7,43–45] Identifying the local energy minimum becomes even more complex for materials with a high defect concentration or a strong electronic perturbation, which can occur upon deep structural reorganization by a chemical reaction, as is the case for metal oxides used in catalysis or fuel cells. Moreover, DFT calculations are not well suited for describing excited states (i.e. the final state with the core hole), requiring further approximations. In this case, finding a reliable structure for the material during or after a reaction (i.e. with an oxygen arrangement valid for all the different atomic environments of the different elements) is extremely ambitious.

To overcome the challenges for materials being measured *in situ*, it is convenient to directly adapt and tune the electronic configuration of untreated samples by means of empirical parameters. In this respect, among the possible DFT codes, the Finite Difference Method Near Edge Structure (FDMNES)[42] program package enables the researcher to directly modify the electronic configuration, allowing to unlock the enigma surrounding the O K-edge.

FDMNES makes use of two empirical parameters, screening and dilatorb,[42] to improve the accuracy of simulating experimental spectra and understanding material properties. The screening parameter addresses the screening of the core hole by a valence electron, which can originate from neighboring parts of the material. This parameter introduces an additional electron from neighboring atoms into the valence orbital of the core-absorbing atom, thereby compensating for possible charge imbalances.[46] Screening is a natural process resulting from the presence of the core hole in the core orbitals of the absorbing atom (1s, 2s, and 2p). The extent of this screening depends on various factors, including material conductivity, the nature of bonds, and the overall electronic structure. The screening parameter, which can range from 0 to 1, reflects the partial electron screening and describes the interaction strength between the absorbing atom and its environment.[42] The dilatorb parameter, on the other hand, controls the radial extent of the valence orbital, particularly the O 2p orbital, from its neutral atomic size.[46] It is associated with the degree of covalency and addresses the actual charge of the oxygen species at the O K-edge.[42] The stronger the covalent character of a bond, the further the valence orbitals expand. On the other hand, strong ionic bonds imply more localized valence orbitals. Together, these parameters allow for a more accurate reproduction of experimental spectra and provide deeper insight into the electronic structure and bonding characteristics of the material (assuming crystallographic structure is unchanged). It must be underlined that the screening and dilatorb parameters are also

applicable to other elements of the periodic table, providing valuable information about the overall properties and reactivity of materials.[46,47]

In this review, we focus on the use of these empirical parameters in O K-edge simulations. This review offers therefore a novel point of view on the topic since it discusses how simple empirical parameters can be used to model quantitatively the experimental data from XAS and XRS and gather important chemical information. As such, it provides a guide on how to observe O K-edge spectra for solid oxide materials used for catalysis and energy applications. The O K-edge measured far from equilibrium can be simulated in the FDMNES scheme using dilatorb and screening, creating a bridge between the experimental fingerprint and the theoretical approaches, thus providing in-depth understanding of the spectra. These parameters are not merely meaningless and arbitrary fitting parameters to achieve a better match with experiments, but they also have a justified physical meaning.

First, a brief overview is provided of the theory that defines the above-mentioned empirical parameters dilatorb and screening. Then, the importance of studying the O K-edge is highlighted, and selected case studies are discussed. The latter illustrates how oxygen K-edge experiments and simulations are an indispensable tool for advancing our understanding of catalytic processes and improving catalyst design, by offering detailed information on the electronic structure, bonding, and real-time changes in (electro)catalysts.

II. Theory.

The FDMNES code

Nowadays, among existing DFT codes, FDMNES is quite a standard code to simulate XAS and XRS spectra, as well as other spectroscopic experimental techniques. It uses the Finite Difference Method (FDM) to avoid the muffin-tin approximation for the potential shape, making the code very precise at the K-edge for all elements and at the $L_{2,3}$-edges of heavier ones. This is a significant advantage of FDMNES compared to other DFT codes, since at these edges, multi-electronic phenomena are sufficiently small to make DFT (under Local Density Approximation, or Perdew-Burke-Ernzerhof approximations) sufficiently precise.

The electronic structure of the material under investigation must be calculated in the entire area probed by the photoelectron by solving the (relativistic) Schrödinger (or Dyson) equation. Hereto, FDMNES uses a cluster approach, considering all the atoms around the absorbing one inside a sphere of a chosen radius, typically between 5 and 7 Å. The electronic structure is most often calculated self-consistently, yielding a final-state potential. From the

latter, using the Fermi Golden rule, one can calculate the electronic states, and thus the projected density of state (pDOS), covering the whole energy range accessible by the spectroscopy in question.

Screening parameter

The oxygen K-edge rises around 530 eV, when a 1s core electron is excited to a partially filled O 2p state (or to a continuum state), leaving behind a core hole in the 1s orbital. The newly generated core hole modifies the electronic configuration, but this modification can partially be countered through rearrangement of the remaining electrons, providing some electronic screening of the core hole. Moreover, oxygen can acquire a higher electron density if the neighboring atoms contribute by transferring charge to oxygen, which will add to more efficient screening. Thus, the core hole screening depends on the interaction of oxygen with the neighboring atoms. This idea of screening is implemented in the FDMNES code by introducing the empirical screening parameter, which modifies the electronic charge in the valence orbital of the excited (absorber/scattered) atom by placing an additional electron in the first un-occupied state, compensating the possible charge imbalance between the neighboring hybridized ions. By convention, the situation where a photoelectron is completely promoted to an unoccupied state and the produced core hole is not stabilized has a corresponding screening value equal to 0. Increasing the value of the screening parameter up to 1 physically implies enhancing the electron transfer from the neighboring atoms, thereby increasing the electron density on the excited atom and gradually screening the core hole. When the 1s electron is excited, the excited atom charge can be approximated as close to +1 in case of “no screening”. The excited atom will however become almost neutral, when the value of the screening parameter is set equal to 1, i.e. “full screening”. The latter means empirically adding an extra charge from the neighbor atoms, usually from a transition metal (TM). The screening parameter, therefore, helps modeling the degree of charge transfer, which can contribute to interpret some of the materials’ properties: acidity or basicity in catalysts, proton uptake in protonic ceramic fuel cells and charge compensation in batteries, all of which can have an important impact on their functionality.[46,48–53]

Fermi’s Golden Rule takes into account the transition of the core electron towards an empty state. This state may be disrupted by the resulting core hole and concomitant screening, either from the remaining electrons of the excited atom or from farther elements in the material. The latter electronic movements are nevertheless considered here as passive. Within this approximation of considering the other electrons frozen, different ways are used to manage the core hole effect. The most straightforward is the full screening scheme where

an extra electron, coming from the neighboring cations, is placed in the first non-occupied level of the excited absorbing atom, containing the core hole. This implies that the atomic charge of the excited is roughly maintained neutral. It is important to note that, when using the self-consistent field (SCF) procedure to ensure convergence of electronic structure calculations to a stable solution, two strategies can be adopted. In the first one, the SCF calculation is performed for the cluster of atoms in the ground state (GS), yielding the exciting atom potential, $V_{a,SCF\text{-}GS}$, as well as the potential throughout the cluster. On top of this XANES/XRS calculation step, a *sudden* approximation is applied, modifying this SCF potential ($V_{a,SCF\text{-}XS,}$) by adding the difference between the excited atom potential, $V_{a,XC}$, and the non-excited ground state potential, $V_{a,GS}$:

$$V_{a,SCF\text{-}XS} = V_{a,SCF\text{-}GS} + V_{a,XC} - V_{a,GS} \ .$$

This is the default way in FDMNES, which, pragmatically, is most often found to yield the best results.[54] In the second strategy, also available in FDMNES, the SCF step already contains the core hole and the extra screening electron. In this case, the XANES/XRS step is performed with the potential directly issued from the SCF procedure. Whatever the strategy, the amount of screening remains an adjustable parameter, ranging from 1 (complete screening) down to 0 (no screening). Note that whatever the screening amount, it will always result in a contraction of all the atomic orbitals. Empirically, several cases have already been demonstrated where partial screening improves the agreement with experimental data.[55] Because of the dipole selection rule, $\Delta\ell$=+/-1, the XAS K-edge photoelectron probes the p level, which hence provides the most important part of the signal. When the latter is the main conduction band state as in oxygen, the sensitivity to screening will be important. In contrast, screening for transition elements rather affects the quadrupole transition, which probes the 3d levels (at low q).

Dilatorb - Orbital dilatation parameter

At the start of FDMNES, more than 20 years ago, the code did not provide self-consistency. Instead, a specific procedure with a sufficiently good potential was used to calculate the states probed by the photoelectron. The orbital shapes, resulting from the program part calculating the electronic structure of a single atom, were compared with results derived from a SCF code, Wien-2k, applied on the material under study. Then, a parameter termed dilatorb or dilatation (or expansion) factor, δ, was used to optimize the overlap of both atomic orbitals. It is important to remark that in practice this parameter modifies the atomic electron density, $\rho_\delta(r)$, from which one calculates the atomic Coulomb potential ($V_{a,coul}(r)$) and the atomic exchange-correlation potential ($V_{a,EC}(r)$), the sum being a new atomic potential, $V_{a,\delta}(r)$

= $V_{a,coul}(r)+ V_{a,EC}(r)$. Finally, the atomic potential $V_a(r)$ is modified by $\Delta V(r) = V_a(r) - V_{a,\delta}(r)$. The main effect of orbital expansion is that this potential becomes more attractive. Since then and up to now, this parameter has not been used anymore because the SCF was more efficient. In the next section it will be seen, however, that it remains nevertheless interesting in some contexts.

Screening and dilatorb parameters in a non-SCF procedure

Self-consistent calculations are, in principle, always better that a non-SCF procedure. Nevertheless, when systems are not at equilibrium, it can be very difficult to mimic the modification of the electronic structure of a material during a chemical transformation, making the SCF approach inefficient. This review focuses on a class of systems far from equilibrium, i.e. under in situ chemical conditions.

In cases where conditions are constantly varying, the two FDMNES parameters, screening as a conventional one and dilatorb (for orbital dilatation) as less common one, may be of help in simulations. Based on the description in previous sections, their main effect is to change the atomic potential of the excited atom. The latter becomes more attractive when the screening value is reduced or when the orbital is expanded, i.e. higher value of the dilatation parameter. Within their value ranges of [0-1], both parameters work in the same direction[46] when comparing the calculated spectra. Minor differences make them, however, not completely equivalent. Ultimately, when agreement between data and simulation becomes satisfying for specific parameter values, the purpose is to understand their meaning in terms of (electro)chemical properties.

III. O K-edge in Catalysis

In the realm of metal oxide catalysts, oxygen forms bonds with the neighboring metal elements in the oxide, being directly involved in e.g. redox capacity or proton exchange during a catalytic process. Consequently, the O K-edge contains a wealth of information concerning *covalency*, orbital overlap, charge transfer along the bond between the oxygen atom and its transition metal neighbors, and through the latter even on oxygen vacancies, all of which significantly impact bulk and macroscopic properties of a material. Moreover, being element-specific, the edge manifests signature features for specific species and serves as a sensitive indicator of alterations in electronic structure following chemical treatments.

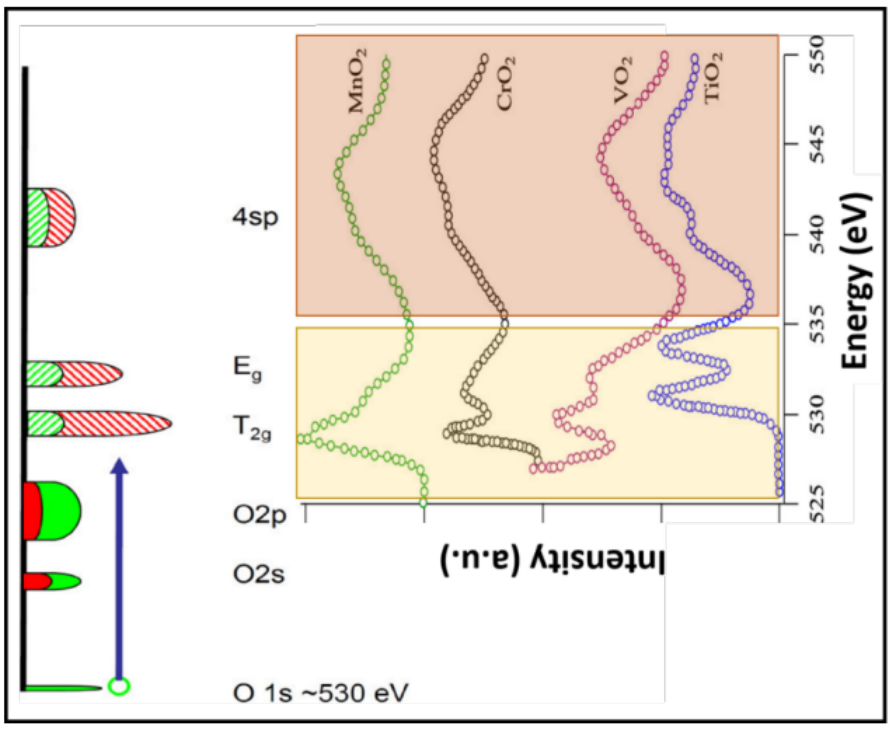

Fig. 1. Interpretation of the oxygen K-edge XAS spectrum for 3d transition metal oxides. The spectrum illustrates the oxygen 1s core state at 530 eV binding energy (green), with occupied oxygen 2s and 2p bands, shown as a mix of oxygen (green) and metal (red) contributions. Unoccupied states are depicted with patterned colors; the t_{2g} and e_g states are in a 6:4 ratio, but have equivalent oxygen contributions (green). At higher energies, the metal 4sp band is represented. The experimental spectra of TiO_2, VO_2, CrO_2, and MnO_2 serve as examples (Open access, adapted from Frati et al. (2020)).[24]

A common approach to visualize the electronic structure of TM oxides is to describe the chemical bonds primarily as bonding between the metal 4sp state and the oxygen p state, forming bonding and antibonding combinations in the valence band. The 3d states also contribute to the chemical bonding, resulting in antibonding valence states. This type of bonding is observed in a (distorted) environment around the TM, leading to the splitting of the 3d states into t_{2g} and e_g states, for O_h local symmetry.[24] Accordingly, in the O K spectra of TM oxides (Fig 1), two distinct regions can be identified: the pre-edge and the main edge (where the resonance occurs).[24,56] The first one corresponds to the oxygen 2p states associated with the empty 3d states of the TM (~525-535 eV). The second in the range of ~535-545 eV is related to transition into the empty 4sp states of the TM.

Analysis of the oxygen K-edge in TM oxides shows that the intensity of the pre-edge region reflects the overlap between ligand 2p and metal 3d orbitals. This overlap helps quantifying the metal-ligand bonding strength, a key concept in understanding lattice oxygen

interactions. The splitting of the 3d band depends on the coordination symmetry of the TM; for example, in an octahedral symmetry around the TM, t_{2g} and e_g orbitals are observed. Differences in position and intensity can be attributed to variations in the occupancy of the t_{2g} and e_g states, impacting interatomic couplings.[56] More generally, the position and shape of the pre-edge can vary depending on the nature of the TM ion, including its oxidation state and d-band occupancy. The bonding strength, associated with the hybridization between the TM and oxygen 2p orbitals, can influence the actual electron charge on the oxygen atom, leading to partial modifications, either increasing or decreasing its charge. Consequently, the pre-edge may shift to either a lower or higher energy position. Additionally, the intensity of the pre-edge reflects the strength of hybridization. Stronger hybridization brings O 2p and TM 3d orbitals closer together, increasing the covalency.

The O K-edge resonance peak typically appearing at a higher energy position (~535-545 eV), corresponds to the metal 4sp band and varies depending on the TM's nature, possible doping, and chemical treatments. This peak also changes with modifications in the electronic structure due to different hybridization and covalency effects.

The following sections showcase the importance of the O K-edge in several different (electro)catalytic applications.

Electrocatalysts

Electrocatalysts play a crucial role in electrochemical reactions by enhancing the rate of oxidation and reduction reactions, at electrode surfaces or within the electrode itself. These catalysts facilitate the electron transfer between electrodes and reactants, as well as intermediate chemical transformations. Fuel cells and electrolyzers represent a prominent application area for electrocatalysts, where efficient electrochemical reactions are vital for energy production. The electronic modification of catalysts involved in electrochemical reactions such as oxygen reduction and oxygen evolution reactions (ORR, OER), can be revealed by investigating the O K-edge.

In a study on the O K-pre-edge of a perovskite (ABO_3)-based material (Fig. 2A) such as $LaBO_3$ (where B = Cr, Mn, Fe, Co, Ni), Suntivich et al.[57] demonstrated a correlation between TM electronegativity, TM-O hybridization, and covalency. $LaNiO_3$ showed higher pre-edge intensity at 530 eV than for perovskites with other TM. This can be linked to electronegativity since across the first-row transition metals to the right of the periodic table at a fixed valence, the transition metal’s electronegativity increases, bringing the 3d orbitals of the metal closer in energy to the 2p orbitals of oxygen. This leads to stronger covalent bonding and enhanced hybridization. A shift in the pre-edge position was also observed in this series of $LaBO_3$.

Similarly, Mueller et al.[58] demonstrated the significance of strong O 2p-TM 3d hybridization in $La_{0.6}Sr_{0.4}FeO_{3-\delta}$ (LSF) and $La_{0.6}Sr_{0.4}Co_{0.2}Fe_{0.8}O_{3-\delta}$ (LSCF). In these mixed-cation perovskites with Fe and Co in the B-site, the pre-edge feature (at ~530 eV), shows splitting due to a change in hybridization, linked to the e_g population upon oxygen incorporation and evolution reactions. This variation highlights the suitability of surface oxygen ions as redox partners in the corresponding chemical treatments.

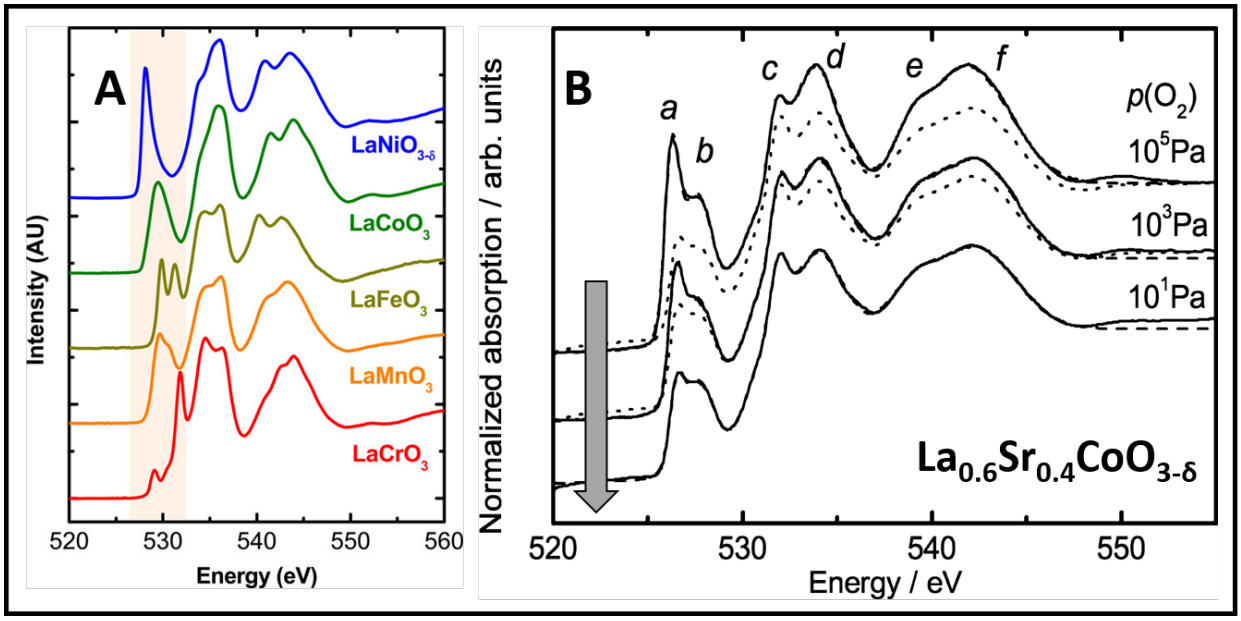

Fig. 2. (A) The increase of the pre-edge intensity at ~ 530 eV and concomitant position shift with increasing electronegativity of the TM in $LaBO_3$ (where B = Cr, Mn, Fe, Co, Ni) (Open access).[57] *(B) The O K-edge XAS spectra of LSC annealed under various partial pressures of oxygen, $p(O_2)$, at 1073 K, where the decreasing pre-edge intensity depicts the oxygen vacancy formation in the Co-O hybridized state (Adapted with permission from J. Phys. Chem. C 2011, 115, 16433–16438).*[59]

Further insights emerged from the O K-edge analysis of $La_{0.6}Sr_{0.4}CoO_{3-\delta}$ (LSC) and LSCF, where the intensity of the pre-edge peak at 527 eV (peak a in Fig. 2B) decreases upon reducing the partial pressure of oxygen, $p(O_2)$, indicating the introduction of oxygen vacancies, which resulted in electron injection into the Co 3d-O 2p hybridized state.[59,60] Under near-OER conditions, EELS revealed surface layer disorder in LSC, alongside reduced Co valence at the surface, which was verified by the observation of a decreased pre-edge intensity at ~530 eV.[61]

Nakamura et al.[62] explored the electronic structural changes in $La_2NiO_{4+\delta}$ during ORR, identifying significant peaks in the O K-edge at 531 eV, corresponding to O_2 molecule

absorption, with the variation in the pre-edge intensity at 530 eV suggesting changes in Ni 3d-O 2p hybridization due to electrochemical polarization.

Other investigations shed light on oxide ion concentration effects, such as those observed in deposited $SrTiO_3$ (STO) and $Nd_{0.5}Sr_{0.5}MnO_3$ (NSMO)/$SrFe_{0.5}Co_{0.5}O_{2.5}$ (SFCO) systems, where higher pre-edge intensities at 528 eV revealed stronger hybridization of O 2p-TM 3d due to higher oxygen content around the TM.[63] Similarly, the high pre-edge at 527.7 eV (Fig. 3A) of hex-$Ba_4Sr_4(Co_{0.8}Fe_{0.2})_4O_{15}$ (BSCF) electrocatalysts unveiled increasing Co valence and robust metal-oxygen covalency.[64]

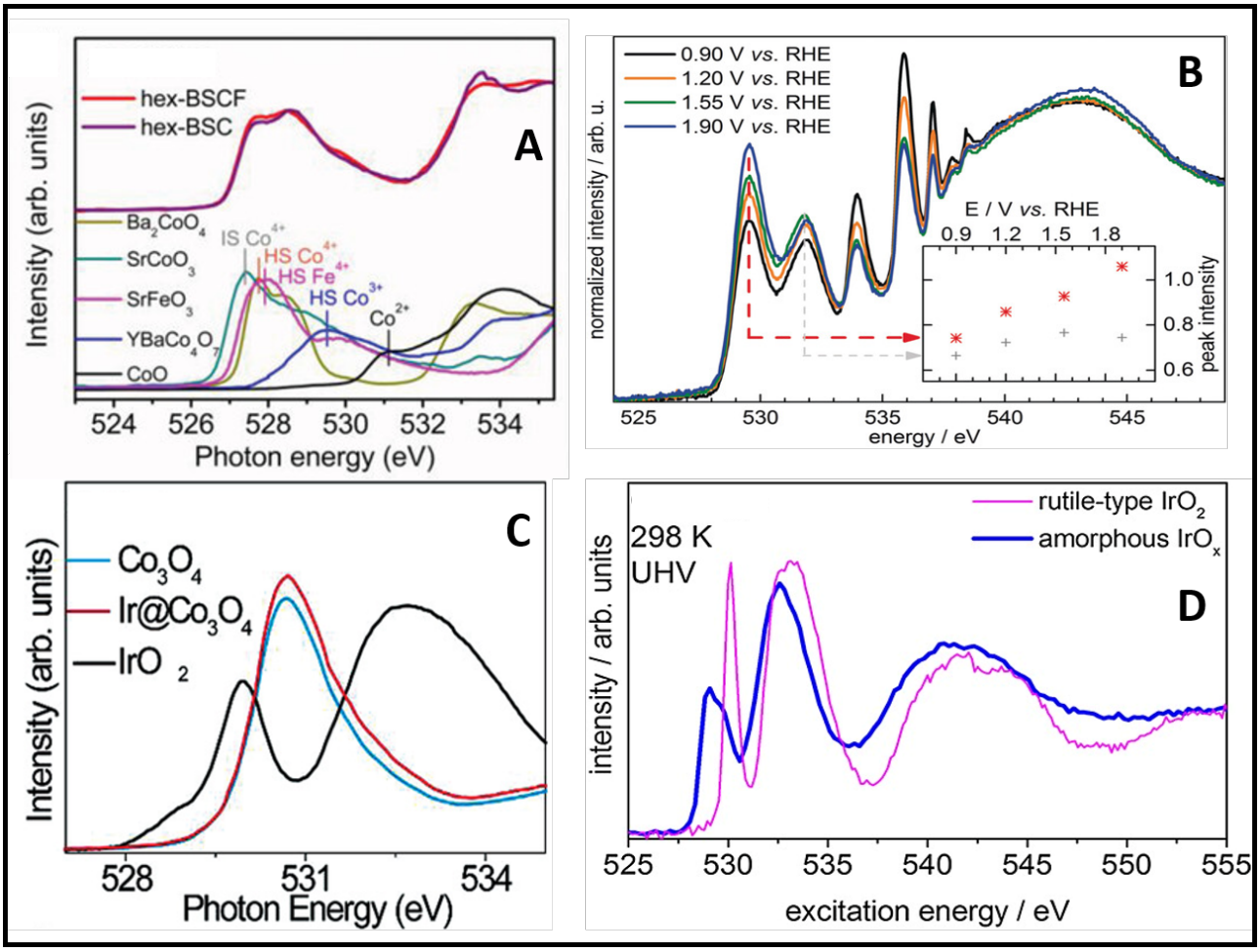

Fig. 3. (A) The O K-edge XAS spectra of hex-BSC ($Ba_4Sr_4Co_4O_{15}$) and hex-BSCF are presented along with several reference materials to indicate the features of the different elements.[64] *(B) Variation in the in situ O K-edge spectra with applied positive potential; the inset shows the intensity at 529 and 532 eV as a function of potential.*[65] *(C) Soft XAS spectrum obtained from Ir/Co_3O_4 compared to reference IrO_2 and Co_3O_4.*[66] *(D) Soft XAS spectra of rutile-type IrO_2 and amorphous IrO_x. In contrast to rutile IrO_2, amorphous IrO_x exhibits an additional pre-edge feature at 529 eV and reduced intensity at 530 eV.* [67] *The figures were adapted with permission.*

In situ soft XAS O K-edge studies on MnO_x electrocatalysts during H_2O electro-oxidation demonstrated increased Mn 3d-O 2p hybridization and Mn-O bond contraction with applied

voltage. The pre-edge at 529 eV (Fig. 3B) increased with applied voltage, whereas the pre-edge at 532 eV remained almost constant, indicating an increase in covalency due to π back-donation from O^{2-} to Mn^{4+}.[65] Similarly, the higher edge intensity at 534 eV and higher intensity ratio of the peaks at 534 and 545 eV obtained from the inner part of layered MnCo2O4/C electrocatalysts revealed the presence of more unoccupied states in the metal.[68] Meanwhile, the insignificant changes at the O K-edge between $V_{0.2}Mo_{0.8}N_{1.2}$ and $MoN_{1.2}$ indicated an unaltered electronic structure of $V_{0.2}Mo_{0.8}N_{1.2}$ compared to $MoN_{1.2}$, confirming no phase separation or transformation occurred upon V doping. [69]

In a similar way, the O K-edge's spectral features of an Ir/Co_3O_4 electrocatalyst (Fig. 3C) for OER mirrored those of Co_3O_4, indicating the electronic structure was unaffected by the presence of Ir.[66] In contrast, comparison between amorphous and rutile-like IrO_2 for OER, measured at room temperature under ultrahigh vacuum, revealed distinct O K-edge peaks at 529 and 530 eV (Fig. 3D), that are attributed to O^- and O^{2-} lattice species in the amorphous phase.[67] In Pt nanorods oriented on Gd-doped ceria electrocatalyst, the decreased O K-edge intensity at 533 eV was attributed to oxygen vacancies resulting from Gd doping and Ce^{4+} to Ce^{3+} conversion.[70] These diverse investigations collectively enrich the understanding of the delicate interplay between TM metal and oxygen.

So far, in these selected pieces of literature mostly the O K-edge was analyzed to understand the metal-oxide interaction and especially to clarify the hybridization between the TM and oxygen. In pioneering works, on the other hand, the hybridization was extensively studied on ideal metal oxide compounds such as MgO, CaO, BaO, or SrO, either by *ab initio* or DFT calculation.[71–76]

Applying the basic DFT procedure in real working systems such as (electro)catalysts is not an easy task. Very often the analysis of the O K-edge is, therefore, solely based on experimental observation, rendering it a qualitative rather than a quantitative approach. However, the concept of screening and dilatorb – the two empirical parameters described previously – allow to overcome the limitations of DFT. Screening simulates the hybridization between O 2p and TM 3d, depicting the nature of the oxide ions and a possible charge transfer along the bond, whereas dilatorb mimics the covalency. The variation in pre-edge and resonance peaks can be reproduced by tuning the values of these two parameters. This approach is much easier than DFT to extract information about the electronic modification, even for a redox-treated system. Application of these two parameters in O K-edge simulations can give direct insight into the macroscopic properties of a system and help unfolding them.

To gain a deeper understanding and extract quantitative information from the O K-edge, Longo et al.[48] extended the work of Orikasa et al.[60] and investigated $La_{0.6}Sr_{0.4}Co_{0.2}Fe_{0.77}Ni_{0.03}O_{3-\delta}$ (LSCF) and Ni-doped LSCF at room temperature by XRS. They were able to reproduce the features of the O K-edge using FDMNES by modifying dilatorb (Fig. 4A, 4B) to model the ionic character of the oxygen bonding to the TM in the structure. They found that a dilatorb value of 0.3 gives the best match for both experimental O K-edge spectra, confirming the increasing oxygen orbital dilatation showing the ability of Ni-doped LSCF to trap the existing oxygen vacancies. In addition, a reduced dilatorb value of 0.0 for undoped LSCF at 800 ºC (Fig. 4B), compared to Ni-doped LSCF, indicates decreased covalency of oxygen, which can be connected to the depletion of the TM 3d orbital and stronger electronic modifications. This study found that Ni insertion helps retaining O 2p-TM 3d hybridization and provides higher stability to the Co environment than in unpromoted LSCF.

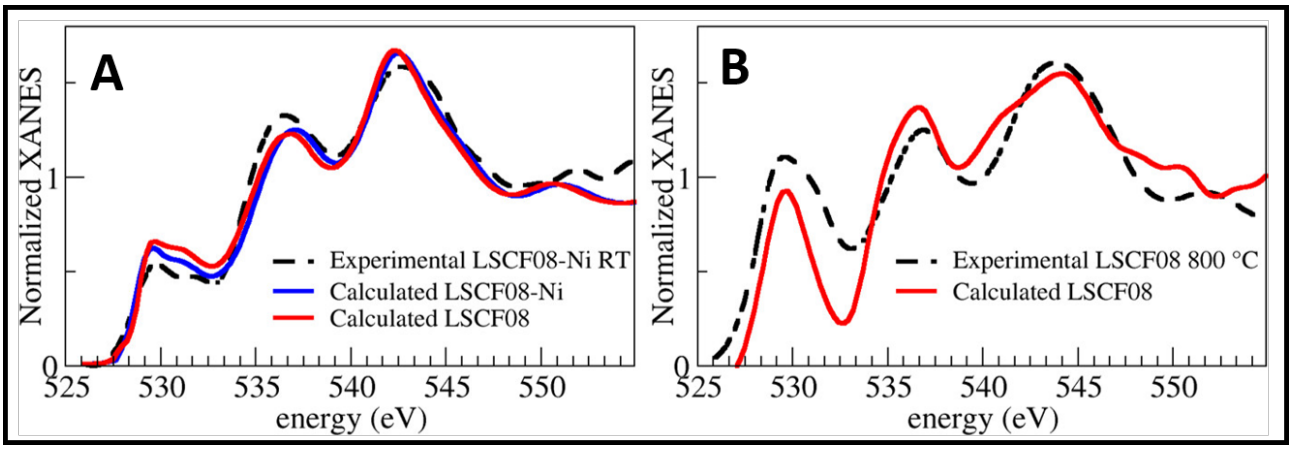

Fig. 4: (A) FDMNES simulation of Ni-doped and undoped LSCF08 with dilatorb value 0.3 versus the experimental LSCF08-Ni data measured at RT.[48] (B) FDMNES simulation of undoped LSCF08 with dilatorb 0.0 versus LSCF08 measured at 800 °C.[48] *The figures were adapted with permission.*

The empirical electronic structure parameters were also used to understand the modifications of protonic ceramic fuel cell (PCFC) materials as a function of cation composition and redox treatments. The perovskite (Ba, Sr, La)(Fe, Zn, Y)$O_{3-\delta}$ serves as PCFC cathode, acting as a mixed conductor of protons, oxygen vacancies, and electron-holes. Raimondi et al.[46] studied the dependence of hole transfer in this perovskite material upon Zn (with oxidation state +2) and Y (having oxidation state +3) doping, partially replacing Fe. They investigated the O K-edge of six materials by XRS: $Ba_{0.95}La_{0.05}FeO_{2.525}$ (BLFred) $Ba_{0.95}La_{0.05}FeO_3$ (BLFox), $BaFe_{0.8}Y_{0.2}O_{2.5}$ (BFYred), $BaFe_{0.8}Y_{0.2}O_{2.9}$ (BFYox), $Ba_{0.95}La_{0.05}Fe_{0.8}Zn_{0.2}O_{2.425}$ (BLFZnred) and $Ba_{0.95}La_{0.05}Fe_{0.8}Zn_{0.2}O_{2.825}$ (BLFZnox); where

'red' denotes the reduced state and 'ox' indicates the oxidized state. The spectral changes in the O K-edge were reproduced by extensive simulations considering both screening and dilatorb. For $BaZrO_3$ (BZ) and BFYox material, the spectra simulated with FDMNES were also compared with DFT simulations (Fig. 5A, 5B), confirming the merit of using appropriately tuned values of screening and dilatorb. To best reproduce the experimental O K-edge for BFYox, and BLFox the required screening values were 0.9 and 0.6, respectively, along with a dilatorb value of 0.1 and 0.15 (Fig. 5B, 5C). The lower screening value for the undoped oxidized sample BLFox than for the Zn- and Y-doped oxidized samples indicates the presence of less negative charge on the oxygen ions for the former, reflecting less charge transfer from TM 3d to O 2p. Lower screening for undoped oxidized samples means less

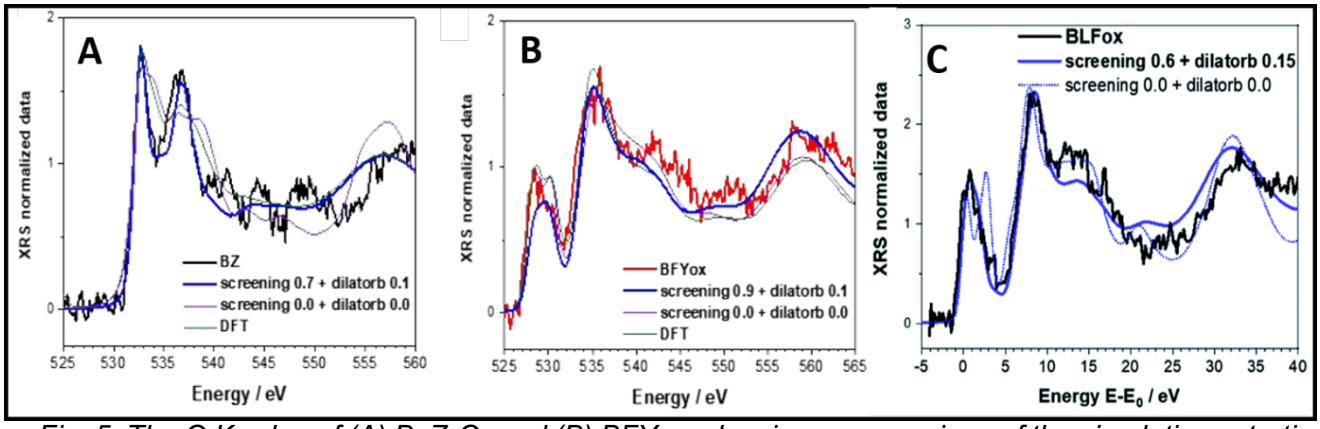

Fig. 5. The O K-edge of (A) $BaZrO_3$ and (B) BFYox. showing a comparison of the simulations starting from the DFT optimized structure, and FDMNES with screening and dilatorb. (C) The simulated O K-edge with a combination of screening and dilatorb for BLFox reproducing in detail the features of the experimental spectra (Open access).[46]

negative charge on oxygen and hence less basicity of the oxygen ions, i.e. making them less prone to donate electrons. Lower screening also reflects a lower proton uptake, as a lower electron density on oxygen means a weaker interaction with protons. For reduced samples BLFred and BLFZred, the simulation with screening and dilatorb values of 0 yielded the best match with the experimental O K-edge (not shown). This points to a lower interaction between TM 3d and O 2p, as well as less overlap for the hybridized TM 3d-O 2p orbitals in the reduced samples.

Another successful attempt of the application of these two parameters was made by Firet et al.,[49] who investigated the surface electronic structure of photocharged (PC) $BiVO_4$ by XRS at the O K-edge (Fig. 6A). This work revealed the formation of a surface layer of bismuth borate with $BiVO_4$, creating a heterojunction during photocharging in a borate electrolyte, which leads to charge separation and charge carrier recombination near the surface. The O

K-edge was reproduced with FDMNES considering the screening and dilatorb parameters (Fig. 6B). Screening values of 0.1 and 0.2 for the dark (without illumination) $BiVO_4$ (bismuth-hydroxide layer) and for the photocharged (with illumination) $BiVO_4$ (bismuth-borate layer), respectively, along with a common dilatorb value of 0.1 reproduced the features of the experimental O K-edge spectra. The difference in screening values between these two samples is attributed to a lower electron density in the conduction band of the photocharged sample. This explains the observed pre-edge filling in the dark sample. The higher screening value in PC-$BiVO_4$ suggests significant structural changes, indicating a shift to a lower Fermi level due to improved band bending induced by the heterojunction between $BiVO_4$ and the surface-formed bismuth borate layer (Fig. 6C). This drives electrons away from the surface, suppressing surface recombination. While both dark and photocharged samples have fewer electrons compared to the reference $BiVO_4$ thin film, the changes are more pronounced in the photocharged sample.

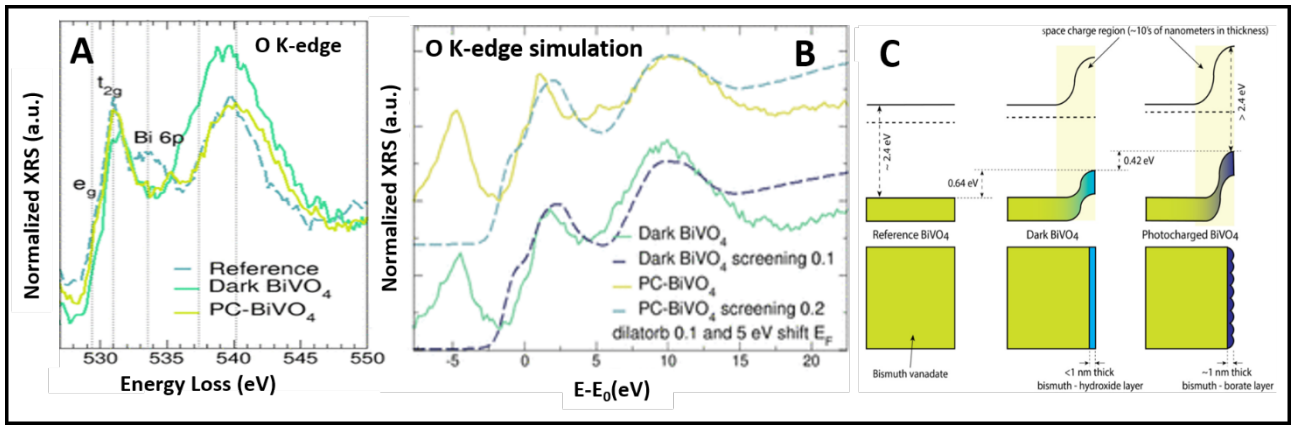

Fig. 6. (A) The normalized XRS spectra depicting the O K-edge regions for a reference ($BiVO_4$ thin film), dark, and PC-$BiVO_4$ sample. The shifting ratio in the contributions to the pre-edge peak indicates its filling with electrons (O 2p-V 3d e_g/t_{2g}) for the dark sample. (B) The O K-edge spectra of both the dark and PC samples are superimposed with FDMNES simulations, incorporating the empirical dilatorb and screening parameters. (C) The schematic diagram shows that photocharging induces changes in the band gap region and Fermi level of $BiVO_4$. The valence band of hydroxide (dark sample) and bismuth borate (PC sample) surface layers lies closer to the Fermi level, resulting in band bending at the surface. This band bending drives electrons towards the bulk of $BiVO_4$, reducing the electron concentration in the space charge region for PC-$BiVO_4$ (Open access).[49]

Heterogeneous Catalysts

The O K-edge is crucial in studies of metal-oxide heterogeneous catalysts because it offers detailed insight into the catalysts' electronic structure and reactivity, which are essential for understanding and therefore optimizing the catalytic performance. Indeed, spectroscopies at this K-edge enable researchers to probe the bonding between oxygen and metal atoms,

potentially comprising the catalytic active sites, offering valuable information about their oxidation state, coordination environment, electron density and phase transitions. From this perspective, quantitative or semiquantitative information, extracted from the O K-edge, is extremely important.

Recent literature in the field of heterogeneous catalysis extensively reports studies involving the comparison of O K-edge data based on experimental observations with reference materials. For instance, Knop-Gericke et al.[77] delved into the intricacies of methanol oxidation to formaldehyde over metallic copper catalysts using high-pressure in situ soft XAS. Through meticulous examination of the O K-edge at varying temperatures, they unveiled a fascinating phase transition from Cu_2O at 540 K to a distinct species where atomic oxygen combines with the s-p bands of copper, instead of the typical hybridization with the Cu d band. Comparison with the spectra of pure Cu_2O at 540 K and 750 K disclosed the presence of both weakly bound surface oxygen and strongly bound bulk oxygen species. Similarly, insights into catalyst modification during CO oxidation to CO_2 were gained by looking at the features of the O K-edge at 530 and 535 eV in CeO_2, revealing a transformation from Ce^{4+} to Ce^{3+} under reduction conditions.[78] Sun et al.[79] further expanded the understanding by investigating the O K-edge of a Ce-Cu_2O catalyst for the CO_2 reduction reaction, where the low-intensity pre-edge at 530.4 eV confirmed the bonding of Ce with O atoms and the spectral shape confirmed the absence of CuO.

On the other hand, experimental data are often coupled with DFT calculations. In this way, quantitative insight into anaerobic CO oxidation was gained from in situ O K-edge and Ce $N_{4,5}$ edge XRS and DFT, showing vacancy ordering in the bulk and explaining modifications at the O K-edge, involving the hybridization of the Ce 4f and 5d and O 2p orbitals.[7] This methodology, based on the comparison of references with data collected at the O K-edge, is also successfully used for other catalysis applications.[80–83]

Exploring the O K-edge through an advanced FDMNES study, which incorporates the screening and dilatorb concept, has opened up a novel avenue for comprehending electronic modifications. Recent investigations[50–52] into heterogeneous catalysts have demonstrated good alignment between the experimental XRS spectrum of the O K-edge and simulations, that consider screening and dilatorb. This approach establishes a link between the oxygen ion nature and the macroscopic properties of the materials, such as basicity or acidity, connecting the oxygen environment to bulk characteristics and properties of oxide materials. For example, Longo et al.[50] investigated the O K-edge of $MgAl_2O_4$, an active catalyst support used for dry reforming of CH_4,[3,84–86] upon high-temperature H_2 reduction. The variation in the simulated O K-edge was shown as a function of screening and dilatorb value (Fig. 7A). A

screening value of 0.7 showed the best match with the experimental O K-edge of fresh $MgAl_2O_4$ catalyst support, whereas a value of 0.8 reproduced the spectral features of reduced $MgAl_2O_4$ (Fig. 7B). In both cases, the applied dilatorb value was 0.1. The higher screening value on oxygen for reduced $MgAl_2O_4$ indicated the tendency of the oxide ions to retain the electron density, reflecting a more confined nature of the electrons in the reduced state.

Tasioula et al.[51] studied 5Fe/10NiMgZr (5 wt.% iron oxide was supported on 10 wt.% NiO-MgO-ZrO_2 mixed oxide), a promising catalyst for CO_2-assisted ethane dehydrogenation (CO_2-EDH). The catalyst was calcined by applying three different conditions: i) at 600 °C for 3h, ii) at 700 °C for 3h, and iii) at 700 °C for 5h, named Fe-600(3h), Fe-700(3h), and Fe-700(5h), respectively. Among these samples, Fe-700(5h) showed the best selectivity towards ethylene production, i.e. 90% at 23.3% C_2H_6 conversion. The authors correlated the ethylene selectivity of Fe-700(5h) to the acidity of the catalyst, based on XRS at the O K-edge and FT-IR spectroscopy during in situ adsorption of pyridine. More specifically, the O K-edge of Fe-700(5h) and Fe-600(3h) were compared (Fig. 7C) and the spectral changes were revealed simulating the screening parameter in FDMNES. Screening values of 0.3 and 0.5 were used for Fe-700(5h) and Fe-600(3h), respectively, along with a default value of the screening parameter of 1 for the reference MgO (see Fig. 7C). The lower value of the screening parameter for Fe-700(5h) indicated less basic oxygen atoms, and hence a higher acidity. The latter increase in acidity was confirmed by in situ adsorption of pyridine followed by FT-IR spectroscopy to measure the respective amount of Lewis and Bronsted acid sites. The bare support 10NiMgZr had less acidity than Fe-600(3h), which depicted that iron incorporation had an impact on the acidity of the catalyst surface. Moreover, the Fe-700(5h) catalyst had four times higher acidity than Fe-600(3h), which is in line with the findings from the O K-edge, i.e. a screening value of 0.3 for Fe-700(5h) vs. 0.5 for Fe-600(3h).

Das et al.[52] followed the same procedure to unfold the nature of oxygen ions in a Ni/$MgFeAlO_4$ dry reforming catalyst, extending the work of Longo.[50] A change in shoulder/main peak ratio was observed in the O K-edge when the catalyst was reduced, re-oxidized, and treated under CH_4:CO_2=1:1 (known as dry reforming of methane, DRM). The

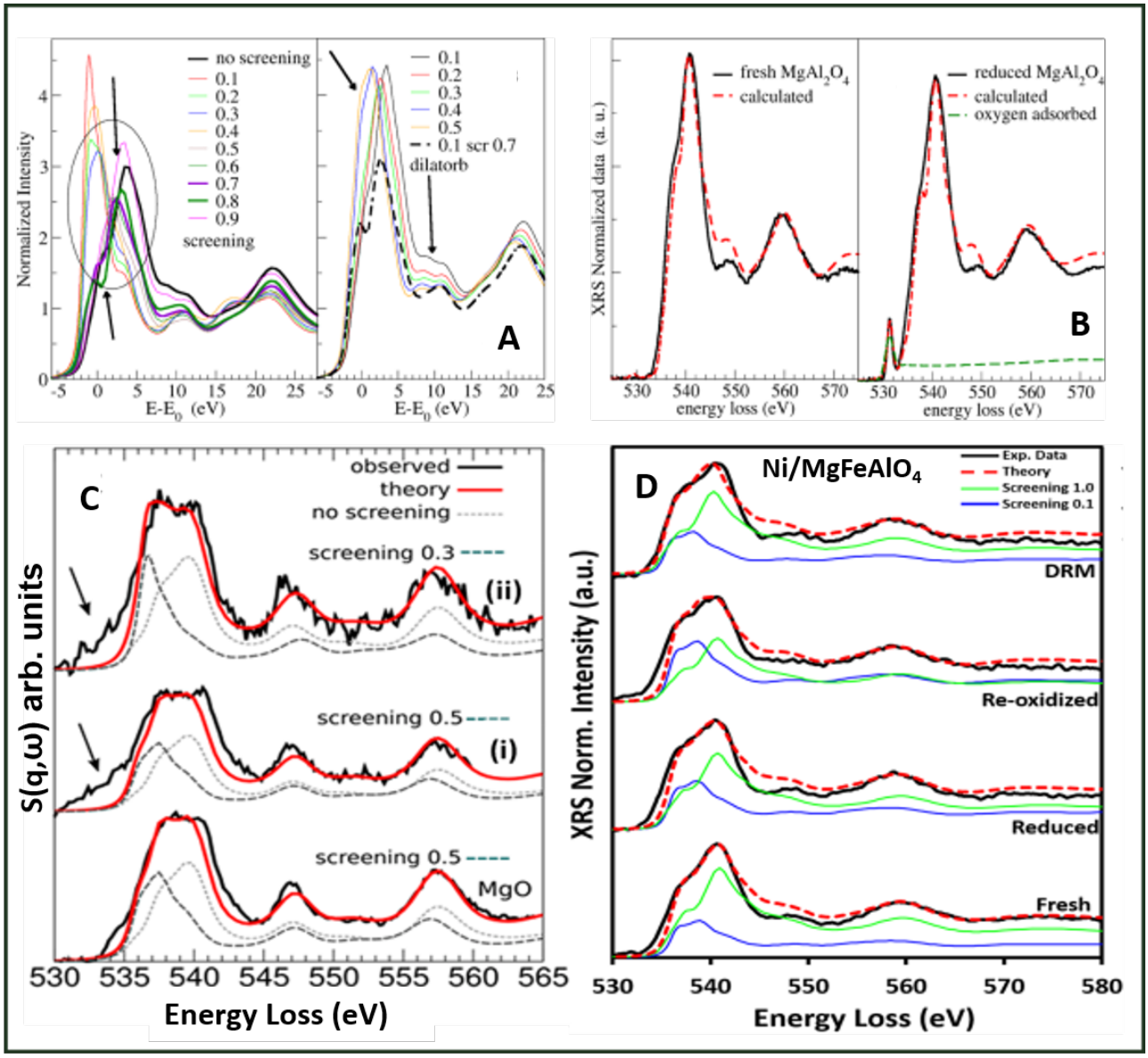

Fig. 7. A) The influence of screening and dilatorb on the computed O K-edge XRS spectrum for $MgAl_2O_4$. Arrows and circles emphasize how varying screening values (left panel) alter the ratio of the feature in the primary edge (without dilatorb parameter). Similarly, the effect of dilatorb is demonstrated (right panel), along with the dash-dot curve that represents a combination of screening and dilatorb.[50] *B) The experimental and calculated spectra at the O K-edge (540 eV) are depicted for fresh (left panel) and reduced $MgAl_2O_4$ (right panel). The green dashed curve represents a molecular oxygen component incorporated into the calculation.*[50] *C) Using screening 1 for reference MgO, the spectra were computed using FDMNES for the following conditions: (i) fresh Fe-600(3h) and (ii) fresh Fe-700(5h). The calculated spectra (red lines) represent the combined contributions of the two components (gray dashed lines) based on their respective screening parameters (Open access).*[51] *(D) Simulation of the O K-edge by a linear combination of two screening values 1.0 and 0.1 shows satisfactory agreement with the experimental spectra of a fresh, reduced, re-oxidized, and*

DRM-treated Ni/MgFeAlO$_4$ catalyst (Open access).[52] *The figures were adapted with permission.*

changes mostly reflected the electronic modification of the support material MgFeAlO$_4$. As the 8wt% Ni content was negligible compared to the support, the simulation was performed considering only the support material. The variation of the O K-edge (Fig. 7D) in the reduced, re-oxidized, and DRM-treated state of the catalyst was reproduced using two different values of the screening parameter in FDMNES: 0.1 and 1.0. The screening parameter provides insight into the acid-base properties of the material, with oxygen atoms acting as Lewis bases when donating electron pairs and Lewis acids when accepting them. While oxygen in oxide materials typically has an oxidation state of -2, making it basic, electron excitation during XRS can formally change its oxidation state to -1, which can further be modified by more or less screening from the neighboring elements. Hence, the increased contribution of screening value of 0.1 after reduction and re-oxidation indicated a higher and therefore less negative, apparent oxidation state of oxygen, suggesting a shift towards more acidic properties.

IV. Battery Materials

Oxygen species are crucial in lithium-based batteries, playing key roles in various components. In oxide- or polyanionic-type cathode materials, oxygen ions interact with Li^+ ions during electrochemical processes. Similar interactions are critical for lithium transport in both polymer and oxide-based solid electrolytes, as well as through SEI layers at the anode-electrolyte interface. In metal-air batteries, molecular oxygen acts as the electrochemically active material, and oxygen redox reactions are also seen in some oxide-based cathodes through anionic redox mechanisms.

Studying the O K-edge in battery systems is essential for understanding these processes, as it provides valuable insights into the local and electronic environment of oxygen species. This includes information on oxidation states, coordination geometry and bonding interactions. This knowledge is essential for elucidating mechanisms such as Li^+ (de)intercalation, oxygen evolution/reduction and structural transformations, all of which affect battery performance, stability and lifespan. By analyzing the O K-edge, researchers can better understand how oxygen species participate in charge transfer, ion diffusion and chemical reactions within battery electrodes and electrolytes, ultimately aiding the design of more efficient, durable, and sustainable battery technologies.

Qiao et al.[87] conducted a comprehensive analysis of the O K-edge for Li_2O, Li_2O_2, and Li_2CO_3, pivotal oxygen-containing species within the SEI, which is crucial for ensuring kinetic stability in Li-ion and Li-air batteries. Their study unveiled distinct variations in the O K-edge spectra, delineating diverse local oxygen environments and showcasing electronic transitions to σ* (O—O) orbital for Li_2O_2 and π*(C=O) orbital for Li_2CO_3. Furthermore, they elucidated the decomposition of Li_2O_2 and Li_2CO_3 into stable LiO_2 species under soft X-ray exposure, highlighting the particular sensitivity of Li_2CO_3.

Several other interesting studies of K-edges concern cathode materials. For instance, during Li^+ (de)insertion, the O K-edge of $Li_{1+x}V_3O_8$ revealed prominent doublets corresponding to transitions to t_{2g} (at 530.1 eV) and e_g (at 531.9 eV) states of vanadium, indicative of larger V 4sp-O 2p hybridization with Li^+ insertion, thereby influencing the bonding geometry.[88] Noteworthy changes in the pre-edge shape and intensity (515-520 eV) of the O K-edge for the layer-structured $Li[Li_{0.15}Ni_{0.275-x}Mg_xMn_{0.575}]O_2$ suggested charge compensation by oxygen ions during the charge-discharge process.[89] This phenomenon was also observed in electrochemically deintercalated $Li_{1-x}CoO_2$, suggesting electron exchange between oxygen and cobalt sites.[90] Van Elp et al.[91] delved into the electronic structure of Li-doped CoO ($Li_xCo_{1-x}O$) and $LiCoO_2$ using O K-edge XAS, revealing compensating holes near Li impurity sites in $Li_xCo_{1-x}O$, with strong hybridization between O 2p holes and Co 3d states leading to a strong antiferromagnetic exchange interaction. In $LiCoO_2$, they observed low-spin Co^{3+} responsible for smaller Co-O distances. Furthermore, significant spectral changes (in both the shape and intensity) of the O K-edge, in the range between 525-530 eV, unveiled the electronic structure of a chemically delithiated $LiCoO_2$ compound, showcasing a higher oxidation state of surface oxygen upon delithiation and indicating different electronic transitions between surface and bulk, suggestive of inhomogeneous delithiation in Li_xCoO_2 compounds.[92]

The use of screening and dilatorb in studies of Li-based battery systems can be beneficial to understand the modifications. Implementation of these two parameters at the O K-edge provides valuable insight in the charge transfer process. In the field of battery studies, however, only a few investigations have, until now, used these parameters to interpret the physico-chemical state of oxygen species. For instance, Fehse et al.[53] studied the charge transfer process of cathode material Li_2FeSiO_4 during one complete electrochemical cycle and probed the O K-edge by XRS to investigate the interaction between anionic O 2p and TM 3d electronic state of Li_2FeSiO_4. The O K-edge spectra obtained for different stages upon charging and discharging are shown in Fig. 8A, where the charge comprises sample A denotes pristine material, D is ‘end of charge’ (EOC), E is ‘EOC + hold’ and the discharge

comprises sample G stands for 'end of discharge' (EOD). The impact of screening and dilatorb were shown in the simulated O K-edge of Li_2FeSiO_4 (Fig. 8 B, C). The O K-edge of sample A and E were reproduced considering screening values of 0.7 and 0.8, respectively with a constant dilatorb value of 0.09 (Fig. 8D). The lower value of screening for sample A implies less O 2p electrons confinement of and hence increased charge sharing of oxygen with TM.

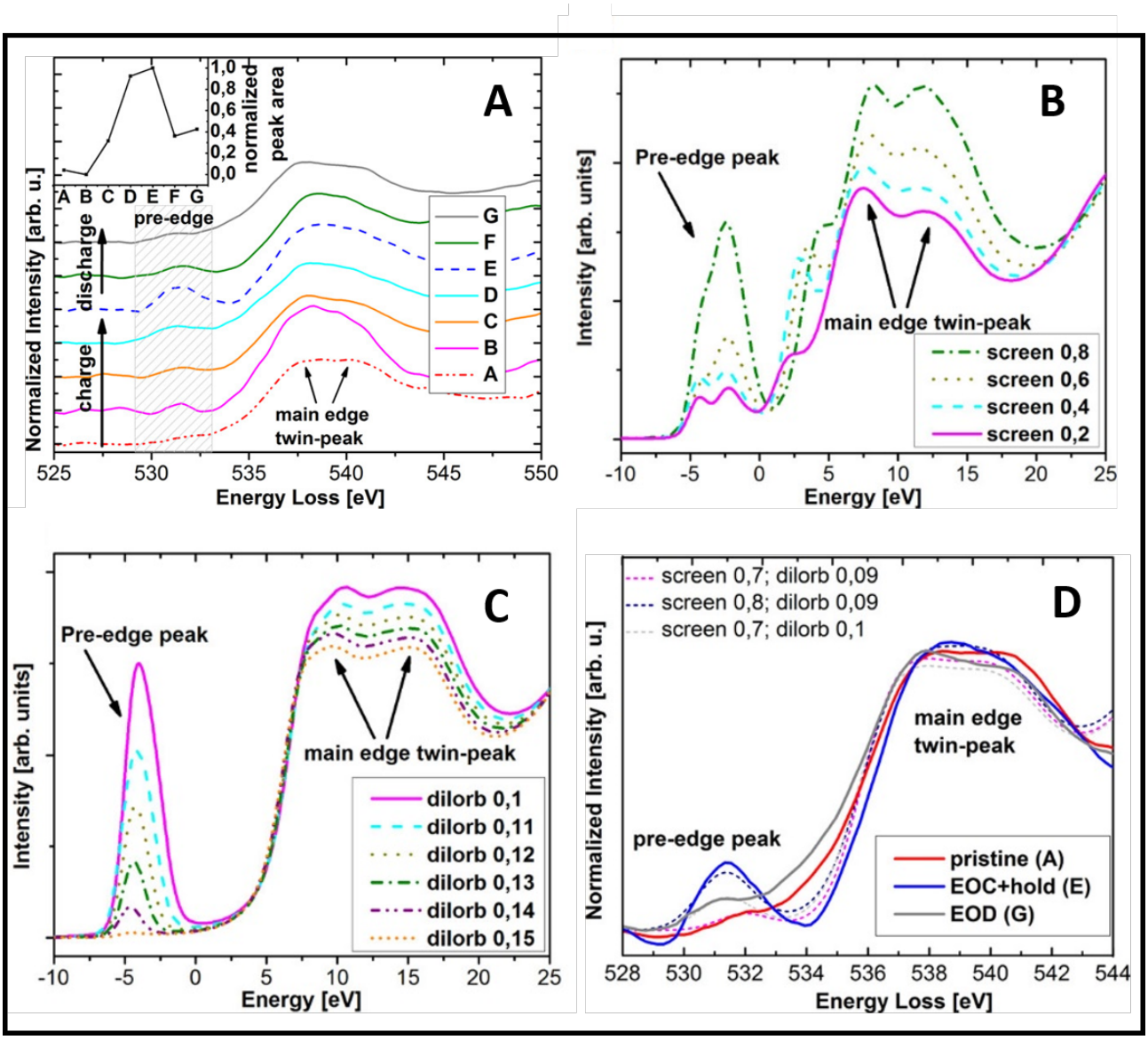

Fig. 8 A) The intensity of O K-edge varies with photon energy loss at various stages along the charge and discharge curve, spectra displayed with vertical offset for clarity. The inset shows the change in the normalized integrated pre-edge peak area (hatched area) corresponding to different positions along the electrochemical cycling curve. B) Influence of screening and C) dilatorb on the simulated O K-edge of Li_2FeSiO_4. D) Experimental spectra (solid lines) and simulated spectra (dotted lines) of the O K-edge for Li_2FeSiO_4 are shown for samples A, E, and G.[53] The figures were adapted with permission.

A similar approach was used to understand the O K-edge spectra of pristine $LiNiO_2$ (LNO), $NaNiO_2$ (NNO), and charged LNO. XRS spectra (Fig. 9, upper panel) indicated enhanced overlap between Ni 3d and O 2p orbitals in charged LNO as observed by the pronounced pre-peak, thereby confirming the increased covalency of the Ni-O bond. To reproduce this feature in FDMNES, a dilatorb value of 0.1 is essential with a screening value of 1.0 (Fig. 9, lower panel). Furthermore, the involvement of oxygen vacancies in charge compensation mechanisms is demonstrated by the Ni-O charge redistribution, which correlates with variations in the screening of oxygen atoms. Hence, a linear combination of two different screening values (1.0 and 0.6) was required to reproduce the O K-edge of charged LNO.[93] However, the simulation was not performed for NNO.

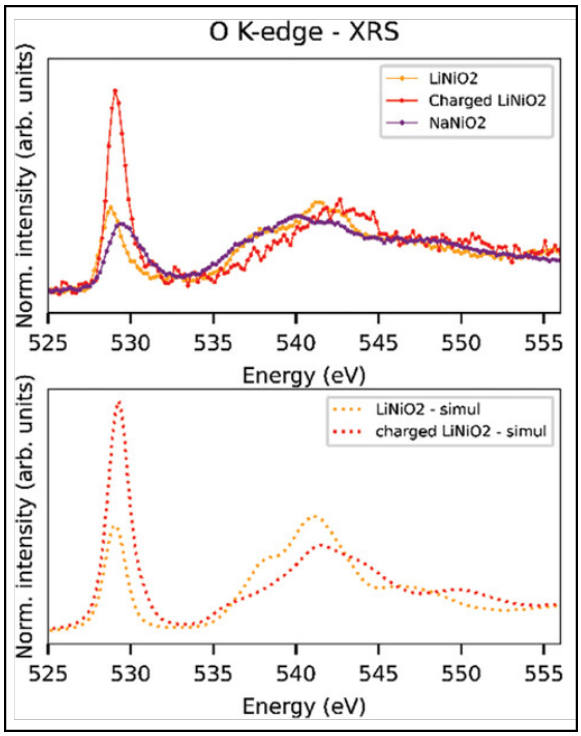

Fig. 9. Upper Panel - The O K-edge spectra of pristine LNO, NNO, and charged LNO are shown. Lower Panel - The O K-edge of $LiNiO_2$ was reproduced using screening = 1 and dilatorb = 0.1 in FDMNES, whereas for charged LNO, two screening values of 1 and 0.6 were required to reproduce the experimental spectrum along with a dilatorb value of 0.1(Adapted with permission).[93]

V. Conclusions and Outlook

The empirical electronic structure parameters screening and dilatorb are pivotal for understanding the intricate electronic behavior of oxygen within metal-oxide systems. In catalysts, oxygen often plays a central role in mediating reactions. The shielding effect of neighboring atoms, which can be understood from the screening parameter, influences the apparent oxidation state of oxygen and its electronic modification, thereby changing its

reactivity as a catalytic species. By comprehensively assessing the screening effect on oxygen, we can gain crucial insight into its role in catalytic processes. Understanding how neighboring atoms modulate the electronic structure around oxygen, sheds light on the interaction of the catalyst with the reactants, having an impact on the catalytic activity and selectivity. Therefore, considering the screening parameter is essential for elucidating the mechanistic details of oxygen-involving catalytic reactions and designing efficient materials tailored for specific applications.

Similarly, this approach can be extended to studies in the realm of electrochemical energy storage, where researchers can gain a deeper understanding of how oxygen species contribute to charge transfer, ion diffusion, and chemical reactions within battery electrodes and electrolytes. This knowledge can ultimately help in designing more efficient, durable, and sustainable battery technologies.

Acknowledgments

Financial support from the French National Research Agency (projects PEPR-Batteries OPENSTORM, ANR-22-PEBA-0005 and Labex STORE-EX, ANR-10-LABX-76-01) is gratefully acknowledged. F.G. acknowledges partial financial support by the European Union - Next Generation EU (componente M4C2, investimento 1.1) through grant PRIN 2022 PNRR P20224RBBX CUP B53D2302745 0001. We acknowledge the European Synchrotron Radiation Facility (ESRF) for provision of synchrotron radiation facilities under proposal numbers IH-CH-1331 and CH-6020.

References

1 V. Muravev, G. Spezzati, Y.-Q. Su, A. Parastaev, F.-K. Chiang, A. Longo, C. Escudero, N. Kosinov and E. J. M. Hensen, Interface dynamics of Pd–CeO2 single-atom catalysts during CO oxidation, *Nat. Catal.*, 2021, **4**, 469–478.

2 S. A. Theofanidis, V. V. Galvita, H. Poelman, R. Batchu, L. C. Buelens, C. Detavernier and G. B. Marin, Mechanism of carbon deposits removal from supported Ni catalysts, *Appl. Catal. B Environ.*, 2018, **239**, 502–512.

3 S. A. Theofanidis, V. V. Galvita, H. Poelman, N. V. R. A. Dharanipragada, A. Longo, M. Meledina, G. Van Tendeloo, C. Detavernier and G. B. Marin, Fe-Containing Magnesium Aluminate Support for Stability and Carbon Control during Methane Reforming, *ACS Catal.*, 2018, **8**, 5983–5995.

4 S. Zaman, L. Huang, A. I. Douka, H. Yang, B. You and B. Y. Xia, Oxygen Reduction

Electrocatalysts toward Practical Fuel Cells: Progress and Perspectives, *Angew. Chemie*, 2021, **133**, 17976–17996.

5 N. Zhang, C. Gao and Y. Xiong, Defect engineering: A versatile tool for tuning the activation of key molecules in photocatalytic reactions, *J. Energy Chem.*, 2019, **37**, 43–57.

6 C. Xie, D. Yan, H. Li, S. Du, W. Chen, Y. Wang, Y. Zou, R. Chen and S. Wang, Defect Chemistry in Heterogeneous Catalysis: Recognition, Understanding, and Utilization, *ACS Catal.*, 2020, **10**, 11082–11098.

7 A. Longo, A. Mirone, E. De Clermont Gallerande, C. J. Sahle, M. P. Casaletto, L. Amidani, S. A. Theofanidis and F. Giannici, Oxygen vacancy clusters in bulk cerium oxide and the impact of gold atoms, *Cell Reports Phys. Sci.*, 2023, **4**, 101699.

8 R. Jin, G. Li, S. Sharma, Y. Li and X. Du, Toward Active-Site Tailoring in Heterogeneous Catalysis by Atomically Precise Metal Nanoclusters with Crystallographic Structures, *Chem. Rev.*, 2021, **121**, 567–648.

9 C. Copéret, A. Comas-Vives, M. P. Conley, D. P. Estes, A. Fedorov, V. Mougel, H. Nagae, F. Núnez-Zarur and P. A. Zhizhko, Surface Organometallic and Coordination Chemistry toward Single-Site Heterogeneous Catalysts: Strategies, Methods, Structures, and Activities, *Chem. Rev.*, 2016, **116**, 323–421.

10 R. Qin, K. Liu, Q. Wu and N. Zheng, Surface Coordination Chemistry of Atomically Dispersed Metal Catalysts, *Chem. Rev.*, 2020, **120**, 11810–11899.

11 V. Muravev, G. Spezzati, Y. Su, A. Parastaev, F. Chiang, A. Longo, C. Escudero, N. Kosinov and E. J. M. Hensen, Interface dynamics of Pd–CeO2 single-atom catalysts during CO oxidation, *Nat. Catal.*, 2021, **4**, 469–478.

12 T. Wang, T. Yang, D. Luo, M. Fowler, A. Yu and Z. Chen, High-Energy-Density Solid-State Metal–Air Batteries: Progress, Challenges, and Perspectives, *Small*, 2024, **20**, 2309306.

13 M. Asmare, M. Zegeye and A. Ketema, Advancement of electrically rechargeable metal-air batteries for future mobility, *Energy Rep.*, 2024, **11**, 1199–1211.

14 R. Cao, J.-S. Lee, M. Liu and J. Cho, Recent Progress in Non-Precious Catalysts for Metal-Air Batteries, *Adv. Energy Mater.*, 2012, **2**, 816–829.

15 M. Li, T. Liu, X. Bi, Z. Chen, K. Amine, C. Zhong and J. Lu, Cationic and anionic redox in lithium-ion based batteries, *Chem. Soc. Rev.*, 2020, **49**, 1688–1705.

16 G. Assat and J.-M. Tarascon, Fundamental understanding and practical challenges of

anionic redox activity in Li-ion batteries, *Nat. Energy*, 2018, **3**, 373–386.

17 M. Ben Yahia, J. Vergnet, M. Saubanère and M.-L. Doublet, Unified picture of anionic redox in Li/Na-ion batteries, *Nat. Mater.*, 2019, **18**, 496–502.

18 R. A. House, J. J. Marie, M. A. Pérez-Osorio, G. J. Rees, E. Boivin and P. G. Bruce, The role of O2 in O-redox cathodes for Li-ion batteries, *Nat. Energy*, 2021, **6**, 781–789.

19 E. Peled and S. Menkin, Review—SEI: Past, Present and Future, *J. Electrochem. Soc.*, 2017, **164**, A1703–A1719.

20 S. Angarita-Gomez and P. B. Balbuena, Lithium-Ion Transport through Complex Interphases in Lithium Metal Batteries, *ACS Appl. Mater. Interfaces*, 2022, **14**, 56758–56766.

21 S. K. Heiskanen, J. Kim and B. L. Lucht, Generation and Evolution of the Solid Electrolyte Interphase of Lithium-Ion Batteries, *Joule*, 2019, **3**, 2322–2333.

22 J. B. Goodenough and P. Singh, Review—Solid Electrolytes in Rechargeable Electrochemical Cells, *J. Electrochem. Soc.*, 2015, **162**, A2387–A2392.

23 H. Yang and N. Wu, Ionic conductivity and ion transport mechanisms of solid-state lithium-ion battery electrolytes: A review, *Energy Sci. Eng.*, 2022, **10**, 1643–1671.

24 F. Frati, M. O. J. Y. Hunault and F. M. F. De Groot, Oxygen K-edge X-ray Absorption Spectra, *Chem. Rev.*, 2020, **120**, 4056–4110.

25 F. M. F. de Groot, M. Grioni and J. C. Fuggle, Oxygen 1s x-ray-absorption, *Phys. Rev. B*, 1989, **40**, 5715–5723.

26 A. Gaur, B. D. Shrivastava and H. L. Nigam, X-Ray Absorption Fine Structure (XAFS) Spectroscopy – A Review, *Proc Indian Natn Sci Acad Spl. Issue, Part B*, 2013, **79**, 921–966.

27 P. Zimmermann, S. Peredkov, P. M. Abdala, S. DeBeer, M. Tromp, C. Müller and J. A. van Bokhoven, Modern X-ray spectroscopy: XAS and XES in the laboratory, *Coord. Chem. Rev.*, 2020, **423**, 213466.

28 C. Colliex, T. Manoubi and O. L. Krivanek, EELS in the electron microscope: A review of present trends, *J. Electron Microsc. (Tokyo).*, 1986, **35**, 307–313.

29 C. Colliex, T. Manoubi and C. Ortiz, Electron-energy-loss-spectroscopy near-edge fine structures in the iron-oxygen system, *Phys. Rev. B*, 1991, **44**, 11402–11411.

30 A. M. Abakumov, S. S. Fedotov, E. V. Antipov and J.-M. Tarascon, Solid state chemistry for developing better metal-ion batteries, *Nat. Commun.*, 2020, **11**, 4976.

31 M. Fehse, A. Iadecola, L. Simonelli, A. Longo and L. Stievano, The rise of X-ray spectroscopies for unveiling the functional mechanisms in batteries, *Phys. Chem. Chem. Phys.*, 2021, **23**, 23445–23465.

32 U. Bergmann, P. Glatzel and S. P. Cramer, Bulk-sensitive XAS characterization of light elements: From X-ray Raman scattering to X-ray Raman spectroscopy, *Microchem. J.*, 2002, **71**, 221–230.

33 U. Bergmann, P. Wernet, P. Glatzel, M. Cavalleri, L. G. M. Pettersson, A. Nilsson and S. P. Cramer, X-ray Raman spectroscopy at the oxygen K edge of water and ice: Implications on local structure models, *Phys. Rev. B - Condens. Matter Mater. Phys.*, 2002, **66**, 1–4.

34 R. Georgiou, C. J. Sahle, D. Sokaras, S. Bernard, U. Bergmann, J.-P. Rueff and L. Bertrand, X-ray Raman scattering: a hard X-ray probe of complex organic systems, *Chem. Rev.*, 2022, **122**, 12977–13005.

35 M. Jaouen, G. Hug, V. Gonnet, G. Demazeau and G. Tourillon, An EELS and XAS Study of Cubic Boron Nitride Synthesized under High Pressure - High Temperature Conditions, *Microsc. Microanal. Microstruct.*, 1995, **6**, 127–139.

36 Z. Wu, G. Ouvrard and P. Gressier, Ti and O K edges for titanium oxides by multiple scattering calculations: Comparison to XAS and EELS spectra, *Phys. Rev. B - Condens. Matter Mater. Phys.*, 1997, **55**, 10382–10391.

37 L. Å. Näslund, D. C. Edwards, P. Wernet, U. Bergmann, H. Ogasawara, L. G. M. Pettersson, S. Myneni and A. Nilsson, X-ray absorption spectroscopy study of the hydrogen bond network in the bulk water of aqueous solutions, *J. Phys. Chem. A*, 2005, **109**, 5995–6002.

38 D. Ketenoglu, A general overview and comparative interpretation on element-specific X-ray spectroscopy techniques: XPS, XAS, and XRS, *X-Ray Spectrom.*, 2022, **51**, 422–443.

39 W. Schülke, *Electron dynamics by inelastic X-ray scattering*, OUP Oxford, 2007, vol. 7.

40 F. M. F. De Groot, H. Elnaggar, F. Frati, R. Wang, M. U. Delgado-jaime, M. Van Veenendaal, J. Fernandez-rodriguez, M. W. Haverkort, R. J. Green, G. Van Der Laan, Y. Kvashnin, A. Hariki, H. Ikeno, H. Ramanantoanina, C. Daul, B. Delley, M. Odelius, M. Lundberg, O. Kuhn, S. I. Bokarev, E. Shirley, J. Vinson, K. Gilmore, M. Stener, G. Fronzoni, P. Decleva, P. Kruger, M. Retegan, Y. Joly, C. Vorwerk, C. Draxl and J. Rehr, 2p x-ray absorption spectroscopy of 3d transition metal systems, *J. Electron Spectros.*

Relat. Phenomena, 2021, **249**, 147061.

41 A. Kotani and H. Ogasawarab, Theory of core-level spectroscopy of rare-earth oxides, *J. Electron Spectros. Relat. Phenomena*, 1992, **60**, 257–299.

42 Y. Joly, C. Cavallari, S. A. Guda and C. J. Sahle, Full-Potential Simulation of X-ray Raman Scattering Spectroscopy, *J. Chem. Theory Comput.*, 2017, **13**, 2172–2177.

43 G. Raimondi, F. Giannici, A. Longo, R. Merkle, A. Chiara, M. F. Hoedl, A. Martorana and J. Maier, X-ray Spectroscopy of (Ba,Sr,La)(Fe,Zn,Y)O3-δIdentifies Structural and Electronic Features Favoring Proton Uptake, *Chem. Mater.*, 2020, **32**, 8502–8511.

44 A. Longo, F. Giannici, M. P. Casaletto, M. Rovezzi, C. J. Sahle, P. Glatzel, Y. Joly and A. Martorana, Dynamic Role of Gold d-Orbitals during CO Oxidation under Aerobic Conditions, *ACS Catal.*, 2022, **12**, 3615–3627.

45 M. F. Hoedl, D. Gryaznov, R. Merkle, E. A. Kotomin and J. Maier, Interdependence of Oxygenation and Hydration in Mixed- Conducting (Ba , Sr) FeO 3 − δ Perovskites Studied by Density Functional Theory, *J. Phys. Chem. C*, 2020, **124**, 11780–11789.

46 G. Raimondi, A. Longo, F. Giannici, R. Merkle, M. F. Hoedl, A. Chiara, C. J. Sahle and J. Maier, Electronic modifications in (Ba, La)(Fe, Zn, Y) O 3− δ unveiled by oxygen K-edge X-ray Raman scattering, *J. Mater. Chem. A*, 2022, **10**, 8866–8876.

47 V. Gulino, A. Longo, L. M. de Kort, H. P. Rodenburg, F. Murgia, M. Brighi, R. Černý, C. J. Sahle, M. Sundermann, H. Gretarsson, F. de Groot and P. Ngene, Anomalous Impact of Mechanochemical Treatment on the Na-ion Conductivity of Sodium Closo-Carbadodecaborate Probed by X-Ray Raman Scattering Spectroscopy, *Small Methods*, 2024, **8**, 2300833.

48 A. Longo, L. F. Liotta, D. Banerjee, V. La Parola, F. Puleo, C. Cavallari, C. J. Sahle, M. Moretti Sala and A. Martorana, The Effect of Ni Doping on the Performance and Electronic Structure of LSCF Cathodes Used for IT-SOFCs, *J. Phys. Chem. C*, 2018, **122**, 1003–1013.

49 N. J. Firet, A. Venugopal, M. A. Blommaert, C. Cavallari, C. J. Sahle, A. Longo and W. A. Smith, Chemisorption of Anionic Species from the Electrolyte Alters the Surface Electronic Structure and Composition of Photocharged BiVO4, *Chem. Mater.*, 2019, **31**, 7453–7462.

50 A. Longo, S. A. Theofanidis, C. Cavallari, N. V. Srinath, J. Hu, H. Poelman, M. K. Sabbe, C. J. Sahle, G. B. Marin and V. V. Galvita, What Makes Fe-Modified MgAl2O4an Active Catalyst Support? Insight from X-ray Raman Scattering, *ACS Catal.*, 2020, **10**, 6613–6622.

51 M. Tasioula, E. de Clermont Gallerande, S. A. Theofanidis, A. Longo, K. A. Lomachenko, C. Sahle and A. A. Lemonidou, Tandem CO2 Valorization and Ethane Dehydrogenation: Elucidating the Nature of Highly Selective Iron Oxide Active Sites, *ACS Catal.*, 2023, **13**, 2176–2189.

52 S. Kumar Das, L. D'ooghe, N. V. Srinath, S. A. Theofanidis, A. Longo, C. Sahle, K. Van Geem, H. Poelman, D. Poelman and V. Galvita, Evolution of Low Z-Elements in a Ni/MgFeAlO4 Catalyst during Reaction: Insight from In Situ XRS, *ACS Catal.*, 2024, **14**, 1311–1323.

53 M. Fehse, C. J. Sahle, M. P. Hogan, C. Cavallari, E. M. Kelder, M. Alfredsson and A. Longo, Bulk-Sensitive Soft X-ray Edge Probing for Elucidation of Charge Compensation in Battery Electrodes, *J. Phys. Chem. C*, 2019, **123**, 24396–24403.

54 O. Bunău and Y. Joly, Self-consistent aspects of x-ray absorption calculations, *J. Phys. Condens. Matter*, 2009, **21**, 345501.

55 Y. Joly, D. Cabaret, H. Renevier and C. R. Natoli, Electron population analysis by full-potential X-ray absorption simulations, *Phys. Rev. Lett.*, 1999, **82**, 2398–2401.

56 J. K. A. Kotani, Core-Level Spectroscopy in Condensed Systems.

57 J. Suntivich, W. T. Hong, Y. L. Lee, J. M. Rondinelli, W. Yang, J. B. Goodenough, B. Dabrowski, J. W. Freeland and Y. Shao-Horn, Estimating hybridization of transition metal and oxygen states in perovskites from o k -edge X-ray absorption spectroscopy, *J. Phys. Chem. C*, 2014, **118**, 1856–1863.

58 D. N. Mueller, M. L. Machala, H. Bluhm and W. C. Chueh, Redox activity of surface oxygen anions in oxygen-deficient perovskite oxides during electrochemical reactions, *Nat. Commun.*, 2015, **6**, 6097.

59 Y. Orikasa, T. Ina, T. Nakao, A. Mineshige, K. Amezawa, M. Oishi, H. Arai, Z. Ogumi and Y. Uchimoto, X-ray absorption spectroscopic study on La0.6Sr 0.4CoO3-δ cathode materials related with oxygen vacancy formation, *J. Phys. Chem. C*, 2011, **115**, 16433–16438.

60 Y. Orikasa, T. Ina, T. Nakao, A. Mineshige, K. Amezawa, M. Oishi, H. Arai, Z. Ogumi and Y. Uchimoto, An X-ray absorption spectroscopic study on mixed conductive La 0.6Sr0.4Co0.8Fe0.2O 3-δ cathodes. I. Electrical conductivity and electronic structure, *Phys. Chem. Chem. Phys.*, 2011, **13**, 16637–16643.

61 M. L. Weber, G. Lole, A. Kormanyos, A. Schwiers, L. Heymann, F. D. Speck, T. Meyer, R. Dittmann, S. Cherevko, C. Jooss, C. Baeumer and F. Gunkel, Atomistic Insights into Activation and Degradation of La0.6Sr0.4CoO3-δElectrocatalysts under Oxygen

Evolution Conditions, *J. Am. Chem. Soc.*, 2022, **144**, 17966–17979.

62 T. Nakamura, R. Oike, Y. Kimura, Y. Tamenori, T. Kawada and K. Amezawa, Operando Soft X-ray Absorption Spectroscopic Study on a Solid Oxide Fuel Cell Cathode during Electrochemical Oxygen Reduction, *ChemSusChem*, 2017, **10**, 2008–2014.

63 J. Lee, Y. Kim, J. Cho, H. Ohta and H. Jeen, Overlayer deposition-induced control of oxide ion concentration in SrFe0.5Co0.5O2.5oxygen sponges, *RSC Adv.*, 2021, **11**, 32210–32215.

64 Y. Zhu, H. A. Tahini, Z. Hu, Z. G. Chen, W. Zhou, A. C. Komarek, Q. Lin, H. J. Lin, C. Te Chen, Y. Zhong, M. T. Fernández-Díaz, S. C. Smith, H. Wang, M. Liu and Z. Shao, Boosting Oxygen Evolution Reaction by Creating Both Metal Ion and Lattice-Oxygen Active Sites in a Complex Oxide, *Adv. Mater.*, 2020, **32**, 1–8.

65 M. F. Tesch, S. A. Bonke, T. E. Jones, M. N. Shaker, J. Xiao, K. Skorupska, R. Mom, J. Melder, P. Kurz, A. Knop-Gericke, R. Schlögl, R. K. Hocking and A. N. Simonov, Evolution of Oxygen–Metal Electron Transfer and Metal Electronic States During Manganese Oxide Catalyzed Water Oxidation Revealed with In Situ Soft X-Ray Spectroscopy, *Angew. Chemie*, 2019, **131**, 3464–3470.

66 Y. Dai, J. Yu, J. Wang, Z. Shao, D. Guan, Y. C. Huang and M. Ni, Bridging the Charge Accumulation and High Reaction Order for High-Rate Oxygen Evolution and Long Stable Zn-Air Batteries, *Adv. Funct. Mater.*, 2022, **32**, 1–9.

67 V. Pfeifer, T. E. Jones, J. J. Velasco Vélez, C. Massué, R. Arrigo, D. Teschner, F. Girgsdies, M. Scherzer, M. T. Greiner, J. Allan, M. Hashagen, G. Weinberg, S. Piccinin, M. Hävecker, A. Knop-Gericke and R. Schlögl, The electronic structure of iridium and its oxides, *Surf. Interface Anal.*, 2016, **48**, 261–273.

68 Y. Yang, Y. Xiong, M. E. Holtz, X. Feng, R. Zeng, G. Chen, F. J. DiSalvo, D. A. Muller and H. D. Abruña, Octahedral spinel electrocatalysts for alkaline fuel cells, *Proc. Natl. Acad. Sci. U. S. A.*, 2019, **116**, 24425–24432.

69 H. Jin, H. Yu, H. Li, K. Davey, T. Song, U. Paik and S. Qiao, MXene analogue: a 2D nitridene solid solution for high-rate hydrogen production, *Angew. Chemie*, 2022, **134**, e202203850.

70 G. Shi, T. Tano, D. A. Tryk, A. Iiyama, M. Uchida, Y. Kuwauchi, A. Masuda and K. Kakinuma, Pt nanorods oriented on Gd-doped ceria polyhedra enable superior oxygen reduction catalysis for fuel cells, *J. Catal.*, 2022, **407**, 300–311.

71 G. Fronzoni, R. De Francesco and M. Stener, Time dependent density functional theory of X-ray absorption spectroscopy of alkaline-earth oxides, *J. Phys. Chem. B*,

2005, **109**, 10332–10340.

72 G. Pacchioni, J. M. Ricart and F. Illas, Ab Initio Cluster Model Calculations on the Chemisorption of CO2and SO2Probe Molecules on MgO and CaO (100) Surfaces. A Theoretical Measure of Oxide Basicity, *J. Am. Chem. Soc.*, 1994, **116**, 10152–10158.

73 G. Pacchioni, C. Sousa, F. Illas, F. Parmigiani and P. S. Bagus, Measures of ionicity of alkaline-earth oxides from the analysis of ab initio cluster wave functions, *Phys. Rev. B*, 1993, **48**, 11573–11582.

74 G. Pacchinoni and P. S. Bagus, Theoretical analysis of the O(1s) binding-energy shifts in alkaline-earth oxides: Chemical or electrostatic contributions, *Phys. Rev. B*, 1994, **50**, 2576–2581.

75 C. Sousa and F. Illas, On the accurate prediction of the optical absorption energy of F-centers in MgO from explicitly correlated ab initio cluster model calculations, *J. Chem. Phys.*, 2001, **115**, 1435–1439.

76 P. S. Bagus, G. Pacchioni, C. Sousa, T. Minerva and F. Parmigiani, Chemical shifts of the core-level binding energies for the alkaline-earth oxides, *Chem. Phys. Lett.*, 1992, **196**, 641–646.

77 A. Knop-Gericke, M. Hävecker, T. Schedel-Niedrig and R. Schlögl, High-pressure low-energy XAS: A new tool for probing reacting surfaces of heterogeneous catalysts, *Top. Catal.*, 2000, **10**, 187–198.

78 D. R. Mullins, S. H. Overbury and D. R. Huntley, Electron spectroscopy of single crystal and polycrystalline cerium oxide surfaces, *Surf. Sci.*, 1998, **409**, 307–319.

79 Y. Sun, J. Xie, Z. Fu, H. Zhang, Y. Yao, Y. Zhou, X. Wang, S. Wang, X. Gao, Z. Tang, S. Li, X. Wang, K. Nie, Z. Yang and Y. M. Yan, Boosting CO2 Electroreduction to C2H4 via Unconventional Hybridization: High-Order Ce4+ 4f and O 2p Interaction in Ce-Cu2O for Stabilizing Cu+, *ACS Nano*, 2023, **17**, 13974–13984.

80 O. A. Makgae, T. N. Phaahlamohlaka, B. Yao, M. E. Schuster, T. J. A. Slater, P. P. Edwards, N. J. Coville, E. Liberti and A. I. Kirkland, Atomic Structure and Valence State of Cobalt Nanocrystals on Carbon under Syngas Versus Hydrogen Reduction, *J. Phys. Chem. C*, 2022, **126**, 6325–6333.

81 Z. Y. Xuze Guan, Hiroyuki Asakura, Rong Han, Siyuan Xu, Hao-Xin Liu, Lu Chen and and F. R. W. Jay Hon Cheung Yan, Tsunehiro Tanaka, Yuzheng Guo, Chun-Jiang Jia, Cascade NH3 Oxidation and N2O Decomposition via Bifunctional Co and Cu Catalysts, *ACS Catal.*, 2013, 235–240.

82 X. Sun, Y. Xu, S. Bai, G. Liu, T. Shen and Y. F. Song, Electronic structure regulation of halogen anion-intercalated MgAl-LDH for highly selective photothermal oxidation of CH4, *Inorg. Chem. Front.*, 2023, **10**, 1769–1774.

83 Z. Gao, L. Cai, C. Miao, T. Hui, Q. Wang, D. Li and J. Feng, Electronic Metal-Support Interaction Strengthened Pt/CoAl-LDHs Catalyst for Selective Cinnamaldehyde Hydrogenation, *ChemCatChem*, 2022, **14**, e202200634.

84 J. Guo, H. Lou, H. Zhao, D. Chai and X. Zheng, Dry reforming of methane over nickel catalysts supported on magnesium aluminate spinels, *Appl. Catal. A Gen.*, 2004, **273**, 75–82.

85 S. A. Theofanidis, V. V. Galvita, H. Poelman and G. B. Marin, Enhanced carbon-resistant dry reforming Fe-Ni catalyst: Role of Fe, *ACS Catal.*, 2015, **5**, 3028–3039.

86 S. M. Kim, P. M. Abdala, T. Margossian, D. Hosseini, L. Foppa, A. Armutlulu, W. Van Beek, A. Comas-Vives, C. Copéret and C. Müller, Cooperativity and dynamics increase the performance of NiFe dry reforming catalysts, *J. Am. Chem. Soc.*, 2017, **139**, 1937–1949.

87 R. Qiao, Y. De Chuang, S. Yan and W. Yang, Soft X-Ray Irradiation Effects of Li2O2, Li2CO3 and Li2O Revealed by Absorption Spectroscopy, *PLoS One*, 2012, **7**, 3–8.

88 H. C. Choi, Y. M. Jung and S. Bin Kim, Characterization of the electrochemical reactions in the Li 1+xV3O8/Li cell by soft X-ray absorption spectroscopy and two-dimensional correlation analysis, *Appl. Spectrosc.*, 2003, **57**, 984–990.

89 Y. K. Sun, M. G. Kim, S. H. Kang and K. Amine, Electrochemical performance of layered Li[Li0.15Ni0.275-xMgxMn0.575]O 2 cathode materials for lithium secondary batteries, *J. Mater. Chem.*, 2003, **13**, 319–322.

90 W. S. Yoon, K. B. Kim, M. G. Kim, M. K. Lee, H. J. Shin, J. M. Lee, J. S. Lee and C. H. Yo, Oxygen contribution on Li-ion intercalation-deintercalation in LiCoO2 investigated by O K-edge and Co L-edge X-ray absorption spectroscopy, *J. Phys. Chem. B*, 2002, **106**, 2526–2532.

91 J. Van Elp, J. L. Wieland, H. Eskes, P. Kuiper, G. A. Sawatzky, F. M. F. De Groot and T. S. Turner, Electronic structure of coo, li-doped coo, and licoo 2, *Phys. Rev. B*, 1991, **44**, 6090.

92 C. H. Chen, B. J. Hwang, C. Y. Chen, S. K. Hu, J. M. Chen, H. S. Sheu and J. F. Lee, Soft X-ray absorption spectroscopy studies on the chemically delithiated commercial LiCoO2 cathode material, *J. Power Sources*, 2007, **174**, 938–943.

93 Q. Jacquet, N. Mozhzhukhina, P. N. O. Gillespie, G. Wittmann, L. P. Ramirez, F. G. Capone, J.-P. Rueff, S. Belin, R. Dedryvère and L. Stievano, A fundamental correlative spectroscopic study on LixNiO2 and NaNiO2, *arXiv Prepr. arXiv2403.18919*.